Full Length Article

Fabrication of sub-5 nm uniform zirconium oxide films on corrugated copper substrates by a scalable polymer brush assisted deposition method

Pravind Yadav [a,*], Sajan Singh [a,*], Nadezda Prochukhan [a], Arantxa Davó-Quiñonero [a], Jim Conway [b], Riley Gatensby [a], Sibu C. Padmanabhan [a], Matthew Snelgrove [c], Caitlin McFeely [c], Kyle Shiel [c], Robert O'Connor [c], Enda McGlynn [b,c], Miles Turner [b], Ross Lundy [a], Michael A. Morris [a,*]

[a] *School of Chemistry, AMBER@CRANN, Trinity College Dublin, Dublin, Ireland*
[b] *National Centre for Plasma Science & Technology, Dublin City University, Dublin, Ireland*
[c] *School of Physical Sciences, Dublin City University, Dublin, Ireland*

ARTICLE INFO

ABSTRACT

We demonstrate a polymer brush assisted approach for the fabrication of continuous zirconium oxide (ZrO_2) films over large areas with high uniformity (pin-hole free) on copper (Cu) substrates. This approach involves the use of a thiol-terminated polymethyl methacrylate brush (PMMA-SH) as the template layer for the selective infiltration of zirconium oxynitrate (ZrN_2O_7). The preparation of a highly uniform covalently grafted polymer monolayer on the Cu substrate is the critical factor in fabricating a metal oxide film of uniform thickness across the surface. Infiltration is reliant on the chemical interactions between the polymer functional group and the metal precursor. A following reductive H_2 plasma treatment process results in ZrO_2 film formation whilst the surface Cu_2O passive oxide layer was reduced to a Cu/Cu_2O interface. Fundamental analysis of the infiltration process and the resulting ZrO_2 film was determined by XPS, and GA-FTIR. Results derived from these techniques confirm the inclusion of the ZrN_2O_7 into the polymer films. Cross-sectional transmission electron microscopy and energy dispersive X-ray mapping analysis corroborate the formation of ZrO_2 layer at Cu substrate. We believe that this quick and facile methodology to prepare ZrO_2 films is potentially scalable to other high-κ dielectric materials of high interest in microelectronic applications.

1. Introduction

The continual reduction in electronic device's size and the challenges associated with top-down photolithography approaches at extreme dimensions together with the increasing complexity [1] of integrated circuitry has created the demand for controlled deposition of nanoscale materials *via* bottom-up rather than physical processes. [2] The development of area-selective deposition (ASD) [2,3] where coating of selected regions of substrate with active materials offers an attractive strategy that eliminates multiple patterning and etching steps used in the photolithography technique. [4] There are other approaches to potentially complement photolithography including block copolymer (BCP) lithography [5–14], as well as ASD techniques. [15–18] These bottom up approaches can be combined with promising processing methods for the selective infiltration [18,19] of active materials such as

metals and dielectrics for the fabrication of future nanoelectronics. [20] A specific goal of our work is the development of ASD combined with polymer infiltration methods to produce highly coherent metal and oxide films and allow successive layers to be built up to create devices without intermediate lithographic steps; pivotal for bottom-up development of architectures. [16]

Several approaches to the ASD technology arena have been explored in the past, including (most frequently) self-assembled monolayers (SAMs) in conjunction with atomic layer deposition (ALD) to demonstrate substrate specific selectivity. Selectivity in area selective deposition, is accomplished by carefully altering the substrate surface chemistry for the controlled deposition of the inorganic materials. [21,22,23] Here, the fabrication of the material patterns relies on the chemical reaction of ALD vapour phase precursors with pre-deposited SAM molecules. Several leading material research groups have

investigated the practicality of SAM molecules. For example, Bent and co-workers demonstrated well-defined techniques to achieve coating on Cu/SiO2 line space patterns. [21,23–26] Chen et al. have demonstrated promising results in the use of SAMs in the selective deposition of high-κ dielectric materials such as HfO2 and ZrO2. [26] However, defects (pinholes) generated by SAMs and the long processing times required for grafting, makes it industrially less favourable. [27].

Unreactive polymer layers, such as poly(methyl methacrylate), [28] poly(imide), [29–30] poly(vinyl pyrrolidone), [31] chemically amplified resists [32–34] and some physical approaches such as plasma treatment [35] have also been investigated as a route to material patterning. Polymers with different end terminating functional groups (commonly called brushes) can be selectively chemically attached to specific surfaces. For instance, amino- and thiol-terminated polymer brushes exhibit a preference for binding with metal surfaces over metal oxides, while hydroxy-terminated polymer brushes are more likely to be deposited on metal oxide surfaces. Our group's previous research has shown that polymer brush films that are covalently grafted can be used to selectively deposit materials onto patterned line spaces for metal layer ASD. [36–37] Chemical grafting (formation of strong covalent or ionic bonds) of brushes, in particular, is regarded as a preferable substrate modification due to its compatibility with a variety of deposition processes. In our previous work, we thoroughly investigated the key parameters governing the grafting process of high quality polymer brushes on silicon substrates. [38–41] This high coverage interfacial polymer brush layer is critical in fabrication of spatially, thick and defect free nanometal oxide films. [42] Various metal oxides (Al2O3, TiO2, CuO and Co3O4) have been successfully infiltrated on grafted polymer brushes using liquid and vapour phase deposition techniques. [3,37–39,43–46] The utilization of readily available salt precursors (as opposed to the need for engineered vapour phase ALD precursors), the simplicity of the processes, and the low cost of liquid aided depositions of inorganic salts are all advantages. Furthermore, as compared to high temperature deposition methods such as sputtering, chemical vapour deposition (CVD), and ALD procedures, the liquid phase technique allows for homogenous coating of materials at moderate temperature. [17,47–48].

In this article, we develop a liquid phase insertion of zirconium oxynitrate (ZrN2O7) on chemically grafted PMMA brushes to develop ZrO2 thin films on a copper substrate. This is demonstration that complex metal oxides can be directly coated onto metals to create insulating films. The fabrication of uniform polymer brush layer was crucial in the infiltration method leading to homogeneous ZrO2 films. Here, we use a hydrogen plasma process in the oxidation of the ZrN2O7 to ZrO2 and removal of the polymer brush layer. Our past studies have suggested that oxidative plasma and calcination can result in oxidation of metal substrates or films in the process and so directly affect the resistance of the substrate. In previous work we have used acetic acid treatments immediately before brush film deposition to reduce the formed copper oxide at the interface. [49] Herein, we successfully achieved both processes in a single step using reductive H2 plasma annealing, which is a highly attractive feature in terms of reduced process complexity. Moreover, the work extends the use of infiltration methods to nontraditional surfaces other than silicon and might find application in integrated circuit manufacture.

2. Experimental section

2.1. Materials

Blank Cu substrates (copper films deposited on silicon wafer substrates using thermal evaporation) were donated by the Intel Corporation Ireland. Thiol end terminated poly (methyl methacrylate) (PMMA-SH) (number average molecular weight, Mn-6.5 X 10^3 kg mol^{-1} and polydispersity index (PDI) 1.3) was purchased from Polymer Source Inc. (Canada) and used without further purification. PMMA-SH was dissolved in toluene and stirred overnight to obtain 0.6% by weight

solution. Zirconium (IV) oxynitrate hydrate (99% purity) and citric acid (ACS reagent > 99.5 %) were purchased from Merck & Co. (Ireland). High performance liquid chromatography grade ethanol, deionised water (ρ = 18.2 MΩ.cm), and toluene (99.99% purity) were purchased from Merck & Co. (Ireland), too, and used as received.

2.2. Substrate surface functionalisation, polymer coating, metal salt infiltration, and hydrogen plasma etching

Fig. 1 schematically shows the experimental approach for the fabrication of ZrO2 films on the Cu substrate. The substrates were first degreased ultrasonically in toluene for 10 min and dried in nitrogen. Organic adsorbents on Cu surface were removed using an oxygen plasma treatment in a barrel Asher for 2 min (40 kHz, 50 W). The Cu substrate was immersed in 1% wt. citric acid solution for 5 min to remove the surface oxide layer and activate the surface, as confirmed by XPS previously. [3] The citric acid treated substrate was then rinsed with water and dried using dry N2 gas. PMMA-SH solutions were spin coated at 3000 rpm for 25 sec. Spin coated samples were immediately annealed at 170 °C for 5 min on a hot plate and subsequently were ultra-sonicated in toluene for 30 min (2 × 15 min) to remove excess physically adsorbed polymer molecules and yield a monolayer coverage of the brush. This monolayer coverage of polymer brush was infiltrated with an ethanolic solution of zirconium oxynitrate (0.4% wt.) via spin coating at 3000 rpm for 25 sec. To achieve a uniform ZrO2 deposit on Cu surface and eliminate grafted polymers, the samples were plasma treated at 200 °C using hydrogen gas.

2.3. Characterisation

The H2 plasma treatment was performed in an Oxford Instruments FlexAL system (base pressure 1 × 10^{-5} mbar). The sample was heated to 200 °C, and 50 sccm of H2 gas was supplied at a pressure of 40 mTorr along at an RF power of 300 W. The sample which was located downstream from the plasma source was processed for 30 min. X-ray photoelectron spectroscopy (XPS) analysis was performed on a Scienta Omicron monochromatic Al Kα X-ray source (base pressure 1 x10^{-8} mbar), equipped with a 128 channel Argus CU detector. The XPS was coupled in-situ to the FlexAl system via a transfer chamber (base pressure 5 x10^{-7} mbar) to allow for the analysis of the plasma processed samples without breaking vacuum. The transfer time between the FlexAL and XPS chambers was approximately 1 min. XPS data analysis was performed using Casa XPS software. The binding energy scale was referenced to the C 1 s peak of adventitious carbon at 284.8 eV. [50] For survey scans, an analyser pass energy was set to 100 eV while a pass energy of 50 eV was used to obtain higher resolution spectra of characteristic core levels.

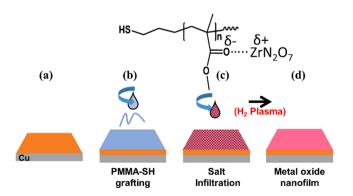A high-resolution field emission scanning electron microscopy (FE-

Fig. 1. Schematic representation of the process for the (a) functionalization of Cu substrate, (b) fabrication of polymer brush film, (c) metal salt inclusion into polymer film (d) reductive polymer ashing and formation of ZrO2 films.

SEM, Carl Ziess ultra) with a secondary electron detector operating at an accelerating voltage of 5 kV was used to acquire top-down images of the samples. Atomic force microscopy (AFM, park system XE7) was used with the non-contact cantilever (AC 160TS, force constant $\sim 26\ nm^{-1}$, resonant frequency ~ 300 kHz).

Dynamic contact angle (CA) measurements (custom built system) equipped with a high-speed camera (60 Hz sampling rate) was used to capture advancing and receding water contact angle on five different regions of each substrate. Water drops were placed at a flow rate of the 5 nL s^{-1} using a 35-gauze needle with droplet volume between 40 and 100 nL.

Grazing -angle Fourier transform infrared (GA-FTIR) was performed using a Nicolet iS50 FTIR Spectrometer equipped with a Harrick Vari-GATR attachment. Prior to sample analysis the germanium crystal was cleaned using butanone before acquiring a background of the atmosphere. Each sample was placed face down on the crystal and a force of approximately 600 N was applied to the sample to ensure sufficient sample-crystal contact. The sample was scanned at an unpolarised angle of incidence of 65° for a total of 128 scans at 8 cm^{-1} resolution.

Transmission electron microscopy (TEM, FEI Osiris) analysis was performed using a bright field and scanning TEM (STEM) imaging, operated at an accelerating voltage of 200 kV. The detector lengths used in STEM were 220, 550, and 770 mm. EDX beam current was 1nA with an acquisition time of 30 min.

3. Results and discussion

3.1. PMMA-SH brush grafting on Cu surface

A description of the results of Cu substrate cleaning in a 1 wt% citric acid solution was described in detail elsewhere. [3,51] XPS data show that the citric acid treatment removes the interfacial oxide layer and activated the surface for further modification (see Figure S1). PMMA-SH dissolved in toluene (0.6% wt.) was coated on the copper substrate immediately after the citric acid treatment and annealed at 170 °C for 5 min. Heat treatment enabled mobility of the polymer chains and rapid reaction between reactive end thiol group and copper metal resulting in the formation of uniform polymer brush on the surface. Contact angle measurements were performed on the grafted brushes together with a control sample (a citric acid treated Cu substrate) for reference. The reference citric acid treated Cu substrate showed an average advancing water contact angle (WCA) of $\theta_{Cu} = 17.45 \pm 2.6°$. After the PMMA-SH brush grafting, the average WCA was recorded to be $\theta_{PMMA} = 75.95 \pm 1.6°$, in close agreement to the value acquired for a pressed homopolymer methyl methacrylate pellet $77.64 \pm 1.4°$ (see Figure S2).

To use the observed θ_a values with surface coverage of the PMMA-SH brush deposited on the copper substrate, we used the Cassie Baxter equation with the assumption of surface energy heterogeneity at the molecular scale [52–53]

$$\Phi = \left(\frac{\cos\theta_{PMMA}}{\cos\theta_{Cu}} - 1\right) \bigg/ \left(\frac{\cos\theta_{PMMA(max)}}{\cos\theta_{Cu}} - 1\right), \qquad (1)$$

Where Φ is the apparent surface coverage of the coated PMMA brush, θ_{PMMA} is the advancing water contact angle (θ_a) of the deposited PMMA-SH brush, θ_{Cu} is the θ_a of the citric acid treated copper substrate, and $\theta_{PMMA(max)}$ is the θ_a of the pressed homopolymer pellet. By solving the above equation, surface coverage of the polymer brush was estimated to be 96% which essentially corresponds to full coverage of the surface within experimental error.

Next, the morphology of the grafted polymer brush film was analysed using a combination of AFM and SEM. It must be noted that solvent washing alone was not effective in removing contamination from the copper substrate (see Figure S3) and cleaning, for example, with long-period aggressive ultrasonication can damage the copper layer. Such an approach was therefore not followed here as a surface cleaning

treatment. For high quality pin-hole free polymer brush grafting, the citric acid treatment was critical prior to brush deposition. This was confirmed by AFM and SEM analysis as shown in Fig. 2a and 2c, respectively, which show that post citric acid treated samples became significantly smoother. Specifically, the root mean square (RMS) roughness value for as received Cu substrate, citric acid treated substrate, and PMMA-SH grafted brushes were calculated to be 5.69 nm (Figure S3), 4.82 nm (Fig. 2a), and 4.71 nm (Fig. 2b), respectively. The RMS value can be used to assess the effectiveness of the polymer brush on the copper surface. Low RMS values observed for the deposited polymer brush correspond to highly regular and uniform film coatings consistent with a single monolayer of the polymer brush and highly coherent pin-hole free films. This can be seen in Fig. 2c and 2d which correspond to SEM images obtained for the citric acid treated and PMMA-SH coated Cu substrate, respectively. The representative SEM images unambiguously show the absence of any micro roughness or irregularities in the polymer brush films formed.

3.2. Fabrication of ZrO$_2$ nanofilm

The grafted PMMA-SH monolayer brush was infiltrated using an ethanolic solution of ZrN$_2$O$_7$ and subsequently converted to ZrO$_2$ nanofilm by H$_2$ reductive plasma annealing. Firstly, the presence of the grafted PMMA was confirmed using XPS. The survey spectrum for the grafted brush showed signals due to C (69.1%), O (28.9%), and Cu (2.0%) as shown in Figure S4a. Following the salt infiltration, C (22.2%) O (60.3%), Cu (9.8%), Zr (5.6%) and N (2.1%) is observed. A reduced in the signal for C is due to the shielding of the bulkier zirconium oxynitrate. Final ZrO$_2$ has the peaks from C (12.0%), O (51.7%), Zr (19.0%) and Cu 2p (17.3%). The C1s peak observed at 288.4 eV confirms the grafting of PMMA brush on copper substrate. Fig. S4b and S4c depicts the survey spectrum for Zr infiltration on copper substrate with and without a deposited PMMA polymer brush, respectively. This shows that the PMMA infiltration is the critical step in film formation. It is observed that without a polymer brush, Zr retention on Cu substrate is significantly less (~0.6 atomic weight %) (Fig. S4b) which we presume is associated with solution droplets not removed during spinning. However, the deposition of the ZrN$_2$O$_7$ solution onto the grafted brushes reveals the inclusion of Zr metal into the PMMA polymer film with retention of 5.6 atomic weight % (see Fig. S4c). Finally, after the H$_2$ plasma treatment the carbon C 1 s signal was significantly reduced to levels typical of adventitious carbon signals and it can be concluded that the hydrogen plasma results in the reductive elimination of the PMMA brush molecules (Fig. S4d). In addition, the H$_2$ plasma treatment causes the polymer to decompose into its volatile components and results in the conversion of zirconium oxynitrate to metallic zirconium. This metallic zirconium is then oxidized to zirconium oxide upon exposure to air. The H$_2$ gas plasma dissociates the H$_2$ molecules into hydrogen atoms, which then react with the polymer to form free radicals. These free radicals subsequently undergo chain scission reactions, producing corresponding monomers and water vapours. In the subsequent step, the H2 plasma reacts with the monomers and dissociates them into volatile fragments. Gupta *et al* [54] demonstrated a similar mechanism for removing the polymer layer using H$_2$ plasma treatment.

The high-resolution XPS spectra for the selected atomic orbitals of C, O, Zr, and Cu from the grafted PMMA brush, metal precursor infiltrated brush and post H$_2$ plasma treated samples were collected and displayed in Fig. 3 (a-d). C 1 s data from the samples containing PMMA brush are fitted into three different components as described by Mani-Gonzalez *et al.* [55] The spectra of C 1 s region for the grafted PMMA-SH film contained three peaks centered at 284.9, 286.6 and 288.8 eV are associated with C–C, C-O-CH$_3$, and O-C=O bonds present in PMMA, respectively (Fig. 3a). [56–57] After the infiltration of ZrN$_2$O$_7$, the carbonyl signal appears to shift from 288.8 to 288.7 eV. This shift may be within experimental error but might also arise from dipole-dipole interactions between the carbonyl oxygen (C = O) and the zirconium ion, as a result
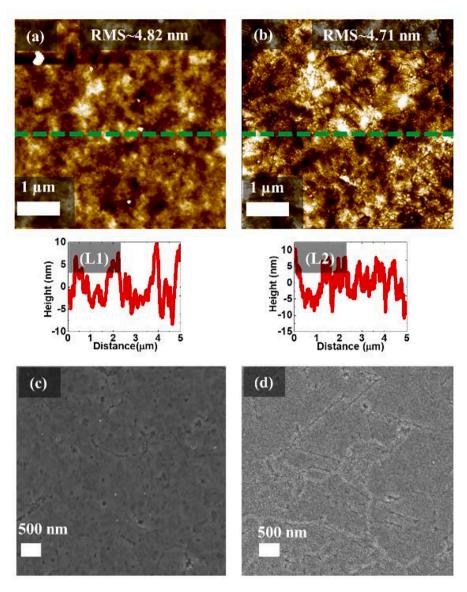
Fig. 2. AFM images of (a) citric acid treated copper substrate (5 min) with line profile at L1, (b) grafted PMMA brush with line profile at L2. (c) and (d) are the respective SEM images of the functionalised Cu substrate and PMMA-SH grafted brush.

of charge transfer from the lone pair of electrons of the oxygen atom to the empty d-orbital of the Zr. [58] After H_2 plasma treatment, the C=O peak of PMMA disappears (within the XPS detection limit), illustrating the complete breakdown of the PMMA into volatile fragments. Additionally, the lower signal-to-noise ratio also reflects the C surface concentration decreased owing to the polymer removal, as displayed in Table S2.

The O 1s XPS spectra shown in Fig. 3b reveal that for the grafted PMMA brush, three different O species can be discerned at 530, 531.8 and 533.5 eV. These peaks are associated with copper(I) oxide, methoxy oxygen and carbonyl oxygen of PMMA. [44,59–60] Intriguingly, following the Zr salt infiltration a negative shift (by -0.5 eV) in the carbonyl oxygen peak is observed, indicating the coordination of the Zr salt into the active site of the polymer as detailed above. Additionally, one extra peak at 532.6 eV is detected, correspond to the nitrate oxygen of ZrN_2O_7. [61] In the post H_2 plasma sample, the polymeric oxygen and copper(I) oxide oxygen signals are absent, while new peak appears at 530.6 eV attributed to the presence of zirconium oxide. [62] The second component at 531.8 eV can be ascribed to the formation of Zr-OH which is typical of air-exposed zirconia surfaces. [63] After the reductive plasma annealing, no measurable nitrate oxide peak is observed,

suggesting the complete conversion of metal precursor to the metal oxide.

The high-resolution Zr 3d spectra in Fig. 3c displays the ZrN_2O_7 infiltrated PMMA-SH brush before and after H_2 plasma exposure. Two peaks for the ZrN_2O_7 infiltrated sample located at 182.1 and 184.6 eV are attributed to the Zr $3d_{5/2}$ and Zr $3d_{3/2}$ spin–orbit peaks, respectively. [64] After the H_2 plasma exposure, a positive shift of + 0.7 eV is observed, which is consistent with the formation of ZrO_2. [65] These results are highly in agreement with the peaks observed in the O 1s region at 530.6 eV, associated to the Zr^{+4} ion. [66] Thus, the data suggest that the oxidation of the Zr nitrate film occurred. The Zr loading present on surface after the reduction process increased by 14 atomic weights % (see Figure S4 and Table S2), consistent with the polymer removal.

Fig. 3d display the Cu 2p XPS spectra for the grafted PMMA brush and the H_2 plasma treated metal infiltrated brush substrate. This region exhibits two peaks for the grafted brush centred at 932.5 and 952.5 eV, respectively, attributed to the Cu $2p_{3/2}$ and Cu $2p_{1/2}$ spin–orbit coupling compounds. [67] A weak satellite peak at ~ 946.2 eV and two minor peaks at 935.2 and 955.2 eV are additionally observed which correspond with the presence of residual CuO. [68] It is suggested that a more
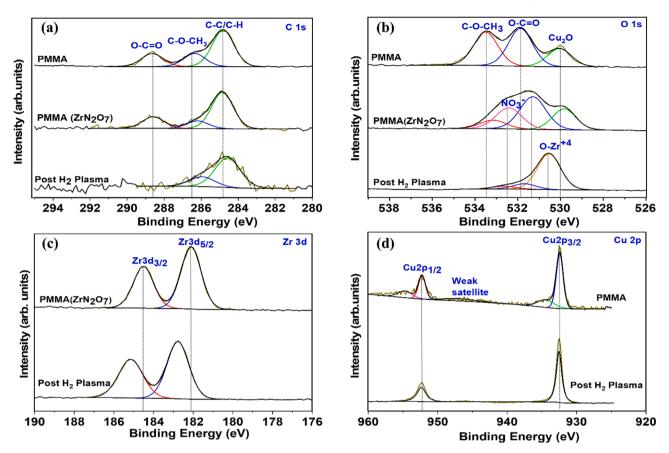
Fig. 3. High-resolution C 1 s and O 1 s (a and b) XPS spectra of the grafted polymer brush, metal infiltrated sample and H_2 plasma annealed substrate, (c) Zr 3d, pre and post plasma treated (d) Cu 2p substrate after the polymer brush grafting and H_2 plasma treatment.
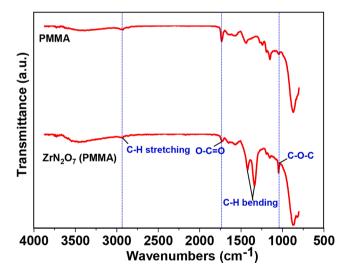

Fig. 4. The FTIR spectra of PMMA and zirconium oxynitrate infiltrated PMMA brush.

oxidized copper oxide species could be formed during the annealing of the polymer brush at 170 °C. The oxidation of the underlying Cu substrate for the grafted brush was further confirmed by Cu LMM peak kinetic energy at 916.6 eV, because this peak is very sensitive to the Cu oxidation state. [69] After the H_2 plasma treatment, the Cu LMM peak shifts back to 919.0 eV and the weak satellite peak and minor peaks are reduced indicating the complete reduction of CuO/Cu_2O to metallic Cu (see Figure S5). This may be important in integrated circuit fabrication because it would improve the electrical conductivity of copper

interconnects.

FTIR analysis further corroborates metal precursor infiltration into polymer brush and its oxidation to metal oxide. The FTIR spectra for grafted PMMA brush and infiltrated ZrN_2O_7 brush is shown in Fig. 4. A strong peak is present at 1734 cm^{-1} in the grafted PMMA brush spectrum and is the characteristic stretching band of the acrylate carbonyl (-C = O) group. [70] Moreover, the peaks observed at 2967, and 2936, cm^{-1} correspond to the C–H stretching vibrations of methyl (–CH_3) and methylene (–CH_2-) groups of PMMA. The peaks located at 1421 and 1336 cm^{-1} are attributed to the bending –C–H vibrations of the –CH_3 group. [71] The peak at 1048 cm^{-1} is associated with the C-O stretching vibration. [72] The FTIR spectra of the grafted PMMA brush can be compared with the ZrN_2O_7 deposited sample. These data reveal a decrease in the acrylate carbonyl band and the increase in intensity for C-O vibration mode in the infiltrated sample. The observed changes can be explained by the coordination of Zr metal ions with the carbonyl unit of the PMMA brush. [73].

The results of the XPS and FTIR analyses suggest that the polymeric carbonyl group and zirconium precursors are bonded via weak dipole–dipole interactions. The decrease in intensity of the carbonyl group in the FTIR spectra of the infiltrated sample could be explained by the carbonyl group being shielded by the bulkier Zr precursors. If there had been a direct covalent bond between zirconium oxynitrate and the polymers, it would have affected the position of the carbonyl band. The dipole–dipole interactions are further supported by the comparison of high-resolution C 1s XPS spectra of the deposited polymer and infiltrated samples.

Fig. 5 shows a representative HAADF-STEM image and the corresponding elemental maps of C, O, Zr, and Cu in H_2 plasma annealed infiltrated PMMA brush sample. Cross-sectional STEM was performed to analyse the zirconium oxide deposition on the copper substrate. The
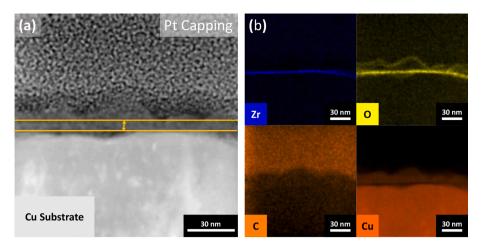
Fig. 5. (a) STEM high-angle annular dark field (HAADF) images of H_2 plasma annealed infiltrated sample, and (b) EDX maps of (Zr, O, C, and Cu).

HAADF-STEM cross-section image in Fig. 5a unambiguously confirms the fabrication of a coherent (i.e. complete coverage) ZrO_2 layer on the Cu substrate of an average thickness ~4 nm thick. The elemental distribution is depicted by EDX mapping data in Fig. 5b. The EDX elemental mapping images show the elemental distribution of the elements Zr, Cu, and O throughout the film. These data indicate several aspects of these films. The zirconia films follow the morphology of the copper surface precisely and are extremely uniform in thickness. However, the TEM lamellae's film preparation caused the 'bumpy' residue at the surface with the thin oxide layer. It can be seen that the copper is free of a surface oxide layer, which is consistent with the XPS data. Furthermore, to strengthen the reliability and consistency of our technique. We scanned multiple regions of the films with the XPS and found essentially identical signals for Zr and other elements. The XPS had a very small spot size, which indicates that a very uniform film is created. In addition, we repeated the deposition process several times and collected the TEM to confirm its homogeneity. The XPS data and TEM image for one of the repetitive samples are shown in the supporting information in Figure S6a and S6b, respectively. We believe that these results demonstrate the reliability and consistency of our technique.

4. Conclusions

In conclusion, we propose a reliable strategy for the infiltration of high-k dielectric precursors into a polymer brush film for the development of high-quality oxide films. This may have considerable importance in selective area deposition technology. We have demonstrated the solvent phase uniform deposition of thiol-terminated PMMA brush coating onto a copper substrate. The liquid phase infiltration technique described can be used to fabricate thin films of zirconium oxide and potentially extended to other important systems such as hafnium oxide. Importantly we have shown that these methods can be extended from silicon wafer substrates to copper metal, which may be important for interconnect technologies in integrated circuit fabrication. This study describes a detailed analysis of the metal infiltration into the polymer brush film. XPS and FTIR analysis of the grafted brush, and infiltrated samples verified the inclusion of the Zr ions into the polymer film. A reductive hydrogen plasma treatment was carried out to eliminate polymer brush and reduce the CuO_x layer formed. The removal of the surface copper oxide during film processing is noteworthy as it provides a low resistance form of thin films for interconnect circuitry. TEM and EDX mapping of the hydrogen plasma treated sample shows that the zirconium oxide is uniformly formed across the substrate, demonstrating that the technique has considerable potential for integration into semiconductor processing and corrosion technologies.

CRediT authorship contribution statement

Pravind Yadav: Methodology, Conceptualization, Investigation, Formal analysis, Visualization, Writing – original draft, Validation. **Sajan Singh:** Methodology, Formal analysis, Investigation, Conceptualization, Writing – review & editing. **Nadezda Prochukhan:** Formal analysis, Writing – review & editing. **Arantxa Davó-Quiñonero:** . **Jim Conway:** Investigation, Writing – review & editing. **Riley Gatensby:** Resources, Formal analysis. **Sibu C. Padmanabhan:** Writing – review & editing. **Matthew Snelgrove:** Investigation, Writing – review & editing. **Caitlin McFeely:** Investigation, Writing – review & editing. **Kyle Shiel:** Methodology, Formal analysis, Writing – review & editing. **Robert O'Connor:** Resources, Conceptualization, Methodology. **Enda McGlynn:** Conceptualization, Methodology, Funding acquisition, Formal analysis, Writing – review & editing. **Miles Turner:** Conceptualization, Methodology, Funding acquisition, Formal analysis, Writing – review & editing. **Ross Lundy:** Formal analysis, Writing – review & editing. **Michael A. Morris:** Resources, Conceptualization, Writing – review & editing, Project administration, Funding acquisition.

Declaration of Competing Interest

The authors declare that they have no known competing financial interests or personal relationships that could have appeared to influence the work reported in this paper.

Data availability

No data was used for the research described in the article.

Appendix A. Supplementary data

Supplementary data to this article can be found online at https://doi.

org/10.1016/j.apsusc.2023.157329.

References

[1] S. Mukesh, J. Zhang, A Review of the Gate-All-Around Nanosheet FET Process Opportunities, Electronics 11 (2022) 3589, https://doi.org/10.3390/electronics11213589.

[2] A.J.M. Mackus, M.J.M. Merkx, W.M.M. Kessels, From the Bottom-Up: Toward Area-Selective Atomic Layer Deposition with High Selectivity †, Chem. Mater. 31 (2019) 2–12, https://doi.org/10.1021/acs.chemmater.8b03454.

[3] C. Cummins, M.T. Shaw, M.A. Morris, Area Selective Polymer Brush Deposition 1700252 (2017) 1–6, https://doi.org/10.1002/marc.201700252.

[4] A.J.M. Mackus, A.A. Bol, W.M.M. Kessels, The use of atomic layer deposition in advanced nanopatterning, Nanoscale 6 (2014) 10941–10960, https://doi.org/10.1039/C4NR01954G.

[5] C. Cummins, A.P. Bell, M.A. Morris, Creating active device materials for nanoelectronics using block copolymer lithography, Nanomaterials 7 (2017), https://doi.org/10.3390/nano7100304.

[6] C. Cummins, M.A. Morris, Using block copolymers as infiltration sites for development of future nanoelectronic devices: Achievements, barriers, and opportunities, Microelectron. Eng. 195 (2018) 74–85, https://doi.org/10.1016/J.MEE.2018.04.005.

[7] R. Lundy, C. Cummins, S.P. Flynn, A. Ghosh, M.N. Collins, E. Dalton, S.M. Kelleher, S. Daniels, M. Morris, R. Enright, Block Copolymer Enabled Nanoporous Membrane Fabrication for High Heat Flux Dissipation Applications, in: Poster Presentation at EMRS Spring Meeting; Lille, France, 2015.

[8] J.Y. Cheng, C.A. Ross, E.L. Thomas, H.I. Smith, G.J. Vancso, Fabrication of nanostructures with long-range order using block copolymer lithography, Appl. Phys. Lett. 81 (2002) 3657–3659, https://doi.org/10.1063/1.1519356.

[9] S.J. Jeong, J.Y. Kim, B.H. Kim, H.S. Moon, S.O. Kim, Directed self-assembly of block copolymers for next generation nanolithography, Mater. Today 16 (2013) 468–476, https://doi.org/10.1016/j.mattod.2013.11.002.

[10] C. Cummins, D. Borah, S. Rasappa, a Chaudhari, T. Ghoshal, B.M.D. O'Driscoll, P. Carolan, N. Petkov, J.D. Holmes, M. a Morris, Self-assembly of polystyrene-block-poly(4-vinylpyridine) block copolymer on molecularly functionalized silicon substrates: fabrication of inorganic nanostructured etchmask for lithographic use, Journal of Materials Chemistry C. 1 (2013) 7941–7951. https://doi.org/Doi 10.1039/C3tc31498g.

[11] C. a Ross, K.K. Berggren, J.Y. Cheng, Y.S. Jung, J.-B. Chang, Three-dimensional nanofabrication by block copolymer self-assembly., Advanced Materials (Deerfield Beach, Fla.). 26 (2014) 4386–96. https://doi.org/10.1002/adma.201400386.

[12] E.C. Giraud, P. Mokarian-Tabari, D.T.W. Toolan, T. Arnold, A.J. Smith, J.R. Howse, P.D. Topham, M.A. Morris, Highly Ordered Titanium Dioxide Nanostructures via a Simple One-Step Vapor-Inclusion Method in Block Copolymer Films, ACS Applied Nano Materials. 1 (2018) 3426–3434, https://doi.org/10.1021/acsanm.8b00632.

[13] M.M.L. Arras, B. He, K.D. Jandt, High molar mass amphiphilic block copolymer enables alignment and dispersion of unfunctionalized carbon nanotubes in melt-drawn thin-films, Polymer 127 (2017) 15–27, https://doi.org/10.1016/j.polymer.2017.08.030.

[14] R. Lundy, S.P. Flynn, C. Cummins, S.M. Kelleher, M.N. Collins, E. Dalton, S. Daniels, M.A. Morris, R. Enright, Controlled solvent vapor annealing of a high χ block copolymer thin film, PCCP 19 (2017) 2805–2815, https://doi.org/10.1039/C6CP07633E.

[15] M.F.J. Vos, S.N. Chopra, M.A. Verheijen, J.G. Ekerdt, S. Agarwal, W.M.M. Kessels, A.J.M. Mackus, Area-Selective Deposition of Ruthenium by Combining Atomic Layer Deposition and Selective Etching, Chem. Mater. 31 (2019) 3878–3882, https://doi.org/10.1021/acs.chemmater.9b00193.

[16] E. Stevens, Y. Tomczak, B.T. Chan, E. Altamirano Sanchez, G.N. Parsons, A. Delabie, Area-Selective Atomic Layer Deposition of TiN, TiO $_2$, and HfO $_2$ on Silicon Nitride with inhibition on Amorphous Carbon, Chemistry of Materials. 30 (2018) 3223–3232. https://doi.org/10.1021/acs.chemmater.8b00017.

[17] A. Mameli, B. Karasulu, M.A. Verheijen, B. Barcones, B. Macco, A.J.M. Mackus, W. M.M.E. Kessels, F. Roozeboom, Area-Selective Atomic Layer Deposition of ZnO by Area Activation Using Electron Beam-Induced Deposition, Chem. Mater. 31 (2019) 1250–1257, https://doi.org/10.1021/acs.chemmater.8b03165.

[18] F.S. Minaye Hashemi, B.R. Birchansky, S.F. Bent, Selective Deposition of Dielectrics: Limits and Advantages of Alkanethiol Blocking Agents on Metal-Dielectric Patterns, ACS Appl. Mater. Interfaces 8 (2016) 33264–33272, https://doi.org/10.1021/acsami.6b09960.

[19] X. Jiang, S.F. Bent, Area-Selective ALD with Soft Lithographic Methods: Using Self-Assembled Monolayers to Direct Film Deposition, J. Phys. Chem. C. 113 (2009) 17613–17625, https://doi.org/10.1021/jp905317n.

[20] R. Chen, Y.C. Li, J.M. Cai, K. Cao, H.B.R. Lee, Atomic level deposition to extend Moore's law and beyond, International Journal of Extreme Manufacturing. 2 (2020), https://doi.org/10.1088/2631-7990/ab83e0.

[21] F. Sadat, M. Hashemi, C. Prasittichai, S.F. Bent, M. Science, C. Engineering, U. S. Present, Self-Correcting Process for High Quality Patterning by Atomic Layer Deposition (2015) 8710–8717, https://doi.org/10.1021/acsnano.5b03125.

[22] G.N. Parsons, R.D. Clark, Area Selective Deposition : Fundamentals, Applications and Future Outlook North Carolina State University, Raleigh NC (2020), https://doi.org/10.1021/acs.chemmater.0c00722.

[23] W.H. Kim, F.S. Minaye Hashemi, A.J.M. Mackus, J. Singh, Y. Kim, D. Bobb-Semple, Y. Fan, T. Kaufman-Osborn, L. Godet, S.F. Bent, A Process for Topographically Selective Deposition on 3D Nanostructures by Ion Implantation, ACS Nano 10 (2016) 4451–4458, https://doi.org/10.1021/acsnano.6b00094.

[24] J.A. Singh, N.F.W. Thissen, W.-H. Kim, H. Johnson, W. (Erwin) M.M. Kessels, A.A. Bol, S.F. Bent, A.J.M. Mackus, Area-Selective Atomic Layer Deposition of Metal Oxides on Noble Metals through Catalytic Oxygen Activation, Chemistry of Materials. (2017) acs.chemmater.7b03818. https://doi.org/10.1021/acs.chemmater.7b03818.

[25] F. Sadat, M. Hashemi, B.R. Birchansky, S.F. Bent, Selective Deposition of Dielectrics: Limits and Advantages of Alkanethiol Blocking Agents on Metal – Dielectric Patterns, (2016). https://doi.org/10.1021/acsami.6b09960.

[26] R. Chen, H. Kim, P.C. McIntyre, S.F. Bent, Self-assembled monolayer resist for atomic layer deposition of HfO2 and ZrO2 high-κ gate dielectrics, Appl. Phys. Lett. 84 (2004) 4017–4019, https://doi.org/10.1063/1.1751211.

[27] C. Vericat, M.E. Vela, G. Benitez, P. Carro, R.C. Salvarezza, Self-assembled monolayers of thiols and dithiols on gold: new challenges for a well-known system (2010), https://doi.org/10.1039/b907301a.

[28] E. Färm, M. Kemell, M. Ritala, M. Leskelä, Selective-area atomic layer deposition using poly(methyl methacrylate) films as mask layers, J. Phys. Chem. C 112 (2008) 15791–15795, https://doi.org/10.1021/jp803872s.

[29] C. Zhang, M. Vehkamäki, M. Pietikäinen, M. Leskelä, M. Ritala, Area-Selective Molecular Layer Deposition of Polyimide on Cu through Cu-Catalyzed Formation of a Crystalline Interchain Polyimide, Chem. Mater. 32 (2020) 5073–5083, https://doi.org/10.1021/acs.chemmater.0c00898.

[30] M. Forouzmehr, S. Zambou, K. Lahtonen, M. Honkanen, R.M. Nazmul Anam, A. Ruhanen, C. Rokaya, D. Lupo, P.R. Berger, Selective atomic layer deposition on flexible polymeric substrates employing a polyimide adhesive as a physical mask, J. Vac. Sci. Technol. A 39 (2021), 012405, https://doi.org/10.1116/6.0000566.

[31] E. Färm, M. Kemell, E. Santala, M. Ritala, M. Leskelä, Selective-Area Atomic Layer Deposition Using Poly(vinyl pyrrolidone) as a Passivation Layer, J. Electrochem. Soc. 157 (2010) K10, https://doi.org/10.1149/1.3250936.

[32] R. Wojtecki, J. Ma, I. Cordova, N. Arellano, K. Lionti, T. Magbitang, T.G. Pattison, X. Zhao, E. Delenia, N. Lanzillo, A.E. Hess, N.F. Nathel, H. Bui, C. Rettner, G. Wallraff, P. Naulleau, Additive lithography−organic monolayer patterning coupled with an area-selective deposition, ACS Appl. Mater. Interfaces 13 (2021) 9081–9090, https://doi.org/10.1021/acsami.0c16817.

[33] A. Sinha, D.W. Hess, C.L. Henderson, A top surface imaging method using area selective ALD on chemically amplified polymer photoresist films, Electrochem. Solid St. 9 (2006), https://doi.org/10.1149/1.2335939.

[34] H.L. Chen, Y.H. Chu, C.I. Kuo, F.K. Liu, F.H. Ko, T.C. Chu, Rapidly selective growth of nanoparticles by electron-beam and optical lithographies with chemically amplified resists, Electrochem. Solid St. 8 (2005) 54–57, https://doi.org/10.1149/1.1845051.

[35] Z. Xiao, K. Kisslinger, S. Chance, S. Banks, Comparison of hafnium dioxide and zirconium dioxide grown by plasma-enhanced atomic layer deposition for the application of electronic materials, Crystals 10 (2020) 1–12, https://doi.org/10.3390/cryst10020136.

[36] C. Cummins, M.T. Shaw, M.A. Morris, Area Selective Polymer Brush Deposition, Macromol. Rapid Commun. 38 (2017) 1700252, https://doi.org/10.1002/marc.201700252.

[37] C. Cummins, T. Weingärtner, M.A. Morris, Enabling Large-Area Selective Deposition on Metal-Dielectric Patterns using Polymer Brush Deactivation, J. Phys. Chem. C 122 (2018) 14698–14705, https://doi.org/10.1021/acs.jpcc.8b04092.

[38] R. Lundy, P. Yadav, A. Selkirk, E. Mullen, T. Ghoshal, C. Cummins, M.A. Morris, Optimizing polymer brush coverage to develop highly coherent sub-5nm oxide films by ion inclusion, Chem. Mater. (2019), https://doi.org/10.1021/acs.chemmater.9b02856.

[39] R. Lundy, P. Yadav, N. Prochukhan, E.C. Giraud, T.F. O'Mahony, A. Selkirk, E. Mullen, J. Conway, M. Turner, S. Daniels, P.G. Mani-Gonzalez, M. Snelgrove, J. Bogan, C. McFeely, R. O'Connor, E. McGlynn, G. Hughes, C. Cummins, M. A. Morris, Precise Definition of a "monolayer Point" in Polymer Brush Films for Fabricating Highly Coherent TiO2Thin Films by Vapor-Phase Infiltration, Langmuir 36 (2020) 12394–12402, https://doi.org/10.1021/acs.langmuir.0c02512.

[40] P. Yadav, R. Gatensby, N. Prochukhan, S.C. Padmanabhan, A. Davó-Quiñonero, P. Darragh, R. Senthamaraikannan, B. Murphy, M. Snelgrove, C. McFeely, S. Singh, J. Conway, R. O'Connor, E. McGlynn, R. Lundy, M.A. Morris, Fabrication of High-κ Dielectric Metal Oxide Films on Topographically Patterned Substrates: Polymer Brush-Mediated Depositions, ACS Appl. Mater. Interfaces. 14 (2022) 32729–32737, https://doi.org/10.1021/acsami.2c07966.

[41] J. Conway, M. Snelgrove, P. Yadav, K. Shiel, R. Lundy, A. Selkirk, R. O'Connor, M. A. Morris, M.M. Turner, S. Daniels, Use of plasma oxidation for conversion of metal salt infiltrated thin polymer films to metal oxide, J. Phys. D: Appl. Phys. 55 (2022), 445206, https://doi.org/10.1088/1361-6463/ac8e12.

[42] M. Snelgrove, C. McFeely, G. Hughes, C. Weiland, J.C. Woicik, K. Shiel, P.G. M. González, C. Ornelas, Ó. Solís-Canto, K. Cherkaoui, P.K. Hurley, P. Yadav, M. A. Morris, E. McGlynn, R. O'Connor, Growth chemistry and electrical performance of ultrathin alumina formed by area selective vapor phase infiltration, Microelectron. Eng. 266 (2022), 111888, https://doi.org/10.1016/j.mee.2022.111888.

[43] M. Snelgrove, C. Zehe, R. Lundy, P. Yadav, J.-P. Rueff, R. O'Connor, J. Bogan, G. Hughes, E. McGlynn, M. Morris, P.G. Mani-Gonzalez, Surface characterization of poly-2-vinylpyridine—A polymer for area selective deposition techniques, J. Vac. Sci. Technol. A 37 (2019), 050601, https://doi.org/10.1116/1.5115769.

[44] P.G. Mani-Gonzalez, M. Snelgrove, J.-P. Rueff, R. Lundy, P. Yadav, J. Bogan, R. O'Connor, M. Morris, G. Hughes, Analysis of Al and Cu salt infiltration into a poly 2- vinylpyridine (P2vP) polymer layer for semiconductor device patterning applications, J. Phys. D Appl. Phys. (2019) 1–20, https://doi.org/10.1088/1361-6463/ab60e8.

[45] M. Snelgrove, C. McFeely, K. Shiel, G. Hughes, P. Yadav, C. Weiland, J.C. Woicik, P.G. Mani-Gonzalez, R. Lundy, M.A. Morris, E. McGlynn, R. O'Connor, Analysing trimethylaluminum infiltration into polymer brushes using a scalable area selective vapor phase process, Materials, Advances 2 (2021) 769–781, https://doi.org/10.1039/d0ma00928h.

[46] C. McFeely, M. Snelgrove, K. Shiel, G. Hughes, P. Yadav, R. Lundy, M.A. Morris, E. McGlynn, R. O'Connor, Rapid area deactivation for blocking atomic layer deposition processes using polystyrene brush layers, J. Mater. Chem. C. 10 (2022) 7476–7484, https://doi.org/10.1039/D2TC00577H.

[47] K. Akiyoshi, T. Kameyama, T. Yamamoto, S. Kuwabata, T. Tatsuma, T. Torimoto, Controlling the oxidation state of molybdenum oxide nanoparticles prepared by ionic liquid/metal sputtering to enhance plasmon-induced charge separation †, (2020). https://doi.org/10.1039/d0ra05165a.

[48] R.D. Clark, Emerging applications for high K materials in VLSI technology, Materials. 7 (2014) 2913–2944, https://doi.org/10.3390/ma7042913.

[49] F.S. Minaye Hashemi, C. Prasittichai, S.F. Bent, Self-Correcting Process for High Quality Patterning by Atomic Layer Deposition, ACS Nano 9 (2015) 8710–8717, https://doi.org/10.1021/acsnano.5b03125.

[50] T.L. Barr, S. Seal, Nature of the use of adventitious carbon as a binding energy standard, J. Vac. Sci. Technol. A 13 (1995) 1239–1246, https://doi.org/10.1116/1.579868.

[51] E.W. Hoppe, A. Seifert, C.E. Aalseth, P.P. Bachelor, A.R. Day, D.J. Edwards, T. W. Hossbach, K.E. Litke, J.I. McIntyre, H.S. Miley, S.M. Schulte, J.E. Smart, G. A. Warren, Cleaning and passivation of copper surfaces to remove surface radioactivity and prevent oxide formation, Nucl. Instrum. Methods Phys. Res., Sect. A 579 (2007) 486–489, https://doi.org/10.1016/j.nima.2007.04.101.

[52] A.B.D. Cassie, S. Baxter, Wettability of porous surfaces, Trans. Faraday Soc. 40 (1944) 546–551.

[53] R. Lundy, C. Byrne, J. Bogan, K. Nolan, M.N. Collins, E. Dalton, R. Enright, Exploring the Role of Adsorption and Surface State on the Hydrophobicity of Rare Earth Oxides, ACS Appl. Mater. Interfaces 9 (2017) 13751–13760, https://doi.org/10.1021/acsami.7b01515.

[54] V. Gupta, N. Madaan, D.S. Jensen, S.C. Kunzler, M.R. Linford, Hydrogen Plasma Treatment of Silicon Dioxide for Improved Silane Deposition, Langmuir 29 (2013) 3604–3609, https://doi.org/10.1021/la304491x.

[55] P.G. Mani-Gonzalez, C. McFeely, M. Snelgrove, K. Shiel, J.A. Hernandez Marquez, R. O'Connor, Titanium infiltration into ultrathin PMMA brushes, J. Vac. Sci. Technol. A 39 (2021), 040403, https://doi.org/10.1116/6.0001061.

[56] G. Beamson, A. Bunn, D. Briggs, High-resolution monochromated XPS of poly (methyl methacrylate) thin films on a conducting substrate, Surface and Interface, Analysis 17 (1991) 105–115, https://doi.org/10.1002/sia.740170206.

[57] C. Ton-That, A.G. Shard, R. Daley, R.H. Bradley, Effects of Annealing on the Surface Composition and Morphology of PS/PMMA Blend (2000), https://doi.org/10.1021/ma000792h.

[58] Y. Kim, A. Bulusu, A.J. Giordano, S.R. Marder, R. Dauskardt, S. Graham, Experimental Study of Interfacial Fracture Toughness in a SiN_x/PMMA Barrier Film, ACS Appl. Mater. Interfaces. 4 (2012) 6711–6719, https://doi.org/10.1021/am301880y.

[59] S. Poulston, P.M. Parlett, P. Stone, M. Bowker, Surface oxidation and reduction of CuO and Cu2O studied using XPS and XAES, Surface and Interface, Analysis 24

(1996) 811–820, https://doi.org/10.1002/(SICI)1096-9918(199611)24:12<811::AID-SIA191>3.0.CO;2-Z.

[60] M. Snelgrove, P.G. Mani-Gonzalez, J. Bogan, R. Lundy, J.P. Rueff, G. Hughes, P. Yadav, E. McGlynn, M. Morris, R. O'Connor, Hard x-ray photoelectron spectroscopy study of copper formation by metal salt inclusion in a polymer film, J. Phys. D Appl. Phys. 52 (2019), https://doi.org/10.1088/1361-6463/ab35b2.

[61] H. Wiame, M.A. Centeno, S. Picard, P. Bastians, P. Grange, Thermal oxidation under oxygen of zirconium nitride studied by XPS, DRIFTS, TG-MS, J. Eur. Ceram. Soc. 18 (1998) 1293–1299, https://doi.org/10.1016/s0955-2219(98)00056-9.

[62] C. Morant, J.M. Sanz, L. Galán, L. Soriano, F. Rueda, An XPS study of the interaction of oxygen with zirconium, Surf. Sci. 218 (1989) 331–345, https://doi.org/10.1016/0039-6028(89)90156-8.

[63] P.C. Wong, Y.S. Li, M.Y. Zhou, K.A.R. Mitchell, XPS investigations of the interactions of hydrogen with thin films of zirconium oxide I. Hydrogen treatments on a 10 Å thick film, Appl. Surf. Sci. 89 (1995) 255–261, https://doi.org/10.1016/0169-4332(95)00031-3.

[64] T. Muneshwar, K. Cadien, Comparing XPS on bare and capped ZrN films grown by plasma enhanced ALD: Effect of ambient oxidation, Appl. Surf. Sci. 435 (2018) 367–376, https://doi.org/10.1016/j.apsusc.2017.11.104.

[65] Y.M. Wang, Y.S. Li, P.C. Wong, K.A.R. Mitchell, XPS studies of the stability and reactivity of thin films of oxidized zirconium, Appl. Surf. Sci. 72 (1993) 237–244, https://doi.org/10.1016/0169-4332(93)90192-E.

[66] P. Lackner, Z. Zou, S. Mayr, U. Diebold, M. Schmid, Using photoelectron spectroscopy to observe oxygen spillover to zirconia, PCCP 21 (2019) 17613–17620, https://doi.org/10.1039/c9cp03322j.

[67] J.P. Espinós, J. Morales, A. Barranco, A. Caballero, J.P. Holgado, A.R. González-Elipe, Interface effects for Cu, CuO, and Cu2O deposited on SiO2 and ZrO2. XPS determination of the valence state of copper in Cu/SiO2 and Cu/ZrO2 catalysts, J. Phys. Chem. B 106 (2002) 6921–6929, https://doi.org/10.1021/jp014618m.

[68] T.M. Ivanova, K.I. Maslakov, A.A. Sidorov, M.A. Kiskin, R.V. Linko, S.V. Savilov, V. V. Lunin, I.L. Eremenko, XPS detection of unusual Cu(II) to Cu(I) transition on the surface of complexes with redox-active ligands, J. Electron Spectrosc. Relat. Phenom. 238 (2020), https://doi.org/10.1016/j.elspec.2019.06.010.

[69] M.C. Biesinger, Advanced analysis of copper X-ray photoelectron spectra, Surface and Interface, Analysis 49 (2017) 1325–1334, https://doi.org/10.1002/sia.6239.

[70] N. Wang, X. Wu, C.S. Liu, Abnormal segmental dynamics of poly(methyl methacrylate)/poly(vinylidene fluoride) blends by mechanical spectroscopy, AIP Adv. 9 (2019), https://doi.org/10.1063/1.5081758.

[71] K.T. Arul, M. Ramanjaneyulu, M.S. Ramachandra Rao, Energy harvesting of PZT/PMMA composite flexible films, Curr. Appl Phys. 19 (2019) 375–380, https://doi.org/10.1016/j.cap.2019.01.003.

[72] J.S. Tu, E. Perevedentseva, P.H. Chung, C.L. Cheng, Size-dependent surface CO stretching frequency investigations on nanodiamond particles, J. Chem. Phys. 125 (2006), https://doi.org/10.1063/1.2370880.

[73] G.T. Hill, D.T. Lee, P.S. Williams, C.D. Needham, E.C. Dandley, C.J. Oldham, G. N. Parsons, Insight on the Sequential Vapor Infiltration Mechanisms of Trimethylaluminum with Poly(methyl methacrylate), Poly(vinylpyrrolidone), and Poly(acrylic acid), J. Phys. Chem. C. 123 (2019) 16146–16152, https://doi.org/10.1021/acs.jpcc.9b02153.